Dimensions and Global Twist of Single-Layer DNA Origami Measured by Small-Angle X-ray Scattering

Dimensions and Global Twist of Single-Layer DNA Origami Measured by Small-Angle X-ray Scattering

Matthew AB Baker[*,1,2], *Andrew J Tuckwell*[*,1], *Jonathan F Berengut*[1], *Jonathan Bath*[3], *Florence Benn*[3], *Anthony P Duff*[4], *Andrew E Whitten*[4], *Katherine E Dunn*[3,5], *Robert M Hynson*[6], *Andrew J Turberfield*[3], *Lawrence K Lee*[^1,6]

[1]European Molecular Biology Laboratory Australia Node for Single Molecule Science, School of Medical Sciences, The University of New South Wales, Sydney, New South Wales, Australia

[2]Current address: School of Biotechnology and Biomolecular Sciences, The University of New South Wales, Sydney, New South Wales, Australia

[3]University of Oxford, Department of Physics, Clarendon Laboratory, Parks Road, Oxford OX1 3PU, UK

[4]Australian Nuclear and Science Technology Organisation, Lucas Heights, New South Wales, Australia,

[5]Current address: School of Engineering, The University of Edinburgh, Edinburgh EH9 3FB

[6]Structural and Computational Biology Division, The Victor Chang Cardiac Research Institute, Darlinghurst, New South Wales, Australia

*These authors contributed equally

[^]Correspondence to: lawrence.lee@unsw.edu.au

KEYWORDS Small-angle X-ray scattering, DNA self-assembly, DNA origami, gold nanoparticles, DNA nanotechnology

GRAPHICAL TABLE OF CONTENTS

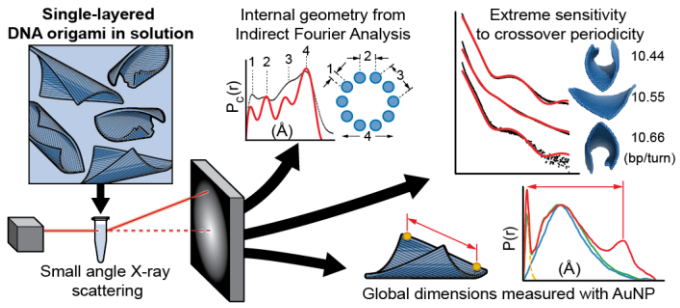

ABSTRACT

The rational design of complementary DNA sequences can be used to create nanostructures that self-assemble with nanometer precision. DNA nanostructures have been imaged by atomic force microscopy and electron microscopy. Small-angle X-ray scattering (SAXS) provides complementary structural information on the ensemble-averaged state of DNA nanostructures in solution. Here we demonstrate that SAXS can distinguish between different single-layer DNA origami tiles that look identical when immobilized on a mica surface and imaged with atomic force microscopy. We use SAXS to quantify the magnitude of global twist of DNA origami tiles with different crossover periodicities: these measurements highlight the extreme structural sensitivity of single-layer origami to the location of strand crossovers. We also use SAXS to quantify the distance between pairs of gold nanoparticles tethered to specific locations on a DNA origami tile and use this method to measure the overall dimensions and geometry of the DNA nanostructure in solution. Finally, we use indirect Fourier methods, which have long been used for the interpretation of SAXS data from biomolecules, to measure the distance between DNA helix pairs in a DNA origami nanotube. Together, these results provide important methodological advances in the use of SAXS to analyze DNA nanostructures in solution and insights into the structures of single-layer DNA origami.

The methods of DNA nanotechnology allow the construction of a wide variety of self-assembling DNA nanostructures with nanometer precision.[1] These include DNA polyhedra,[2-4] DNA tiles,[5,6] DNA boxes,[7] DNA tweezers,[8] molecular walkers,[8-11] robots,[12] cogged gears[13] and 3D structures that reproducibly change arrangements many times over multiple days.[14] DNA nanostructures were first imaged with atomic force microscopy (AFM), which generates three-dimensional maps of surfaces through mechanical probing with a sharp tip.[15] AFM provided verification of several seminal approaches to the design of DNA nanostructures including 2D tile arrays,[5] the high-yield, single-step synthesis of a DNA tetrahedron,[4] and DNA origami,[6] a robust method for folding long, single stranded DNA into 2D and 3D shapes.[16] More recently, transmission electron microscopy (TEM) has emerged as another important method for imaging DNA nanostructures.[13,16-21] One benefit of TEM is that it avoids the deformation or damage of samples that can result from the mechanical interaction with an AFM tip. Moreover, structures can either be imaged on a surface, typically using an electron-dense stain as a contrast agent, or whilst cryogenically frozen and suspended in a thin layer of vitreous ice (cryo-EM). Cryo-EM avoids difficulties in surface-based imaging: nanostructures are captured in their native, hydrated state without the need for contrast agents.[22] Image-averaging methods allow high-resolution (sub-nanometer) structural characterization including 3D shape reconstructions. The 3D structures of a handful of DNA nanostructures have been elucidated through the use of cryo-EM,[3,7,20,21,23,24] with structures of the DNA tetrahedron[20] and a rigid multi-layer DNA origami object[21] determined at resolution sufficient to reveal the structure of the double helix. A majority of DNA nanostructures however, have been imaged with negative-stain TEM or AFM. Both require the deposition of ‘soft’ biomolecules onto a surface: this can deform their structure, especially in the case of single-layer DNA origami.

The archetypal DNA origami tile consists of 26 DNA helices that form a 'log-raft' type structure.[6] The tile is assembled from one long, single-stranded DNA scaffold, derived from the M13 bacteriophage genome, which is folded and held together by short, complementary DNA 'staples' that cross over between helices (Figure 1A). These crossovers are designed to occur where DNA strands from neighbouring helices are in close proximity (Figure 1B). For a flat DNA tile, the spacing between crossovers that link a given pair of helices is constrained to be a multiple of the periodicity of the double helix, approximately 10.5 base pairs (bp)/turn[13] (Figure 1B-D). In practice, however, it is not always possible for crossover locations to strictly correspond to the periodicity of DNA. Indeed, the original DNA origami tile had an average crossover periodicity corresponding to 10.66 bp/turn (Figure. 1E) and consequently is thought to be twisted because helices would be under-wound if the tile were forced to be flat. Yet this tile appears flat when imaged with AFM.[6] Conversely, where the crossover periodicity is less than the periodicity of a double helix, it is possible to assemble DNA origami structures that are twisted in the opposite direction (Figure 1F). Such global twists are observable in TEM micrographs of multi-layer origami structures where crossover periodicities deviate substantially (*e.g.* 10.0 bp/turn) from the periodicity of a DNA duplex.[13] Since the global twist of a DNA origami structure depends not only on the crossover periodicity but also the torsional and bending stiffness of the structure, the effect of altering crossover periodicity on the global twist of single-layer DNA nanostructures is expected to be more pronounced than in multi-layer origami structures, but this has not yet been experimentally characterized.

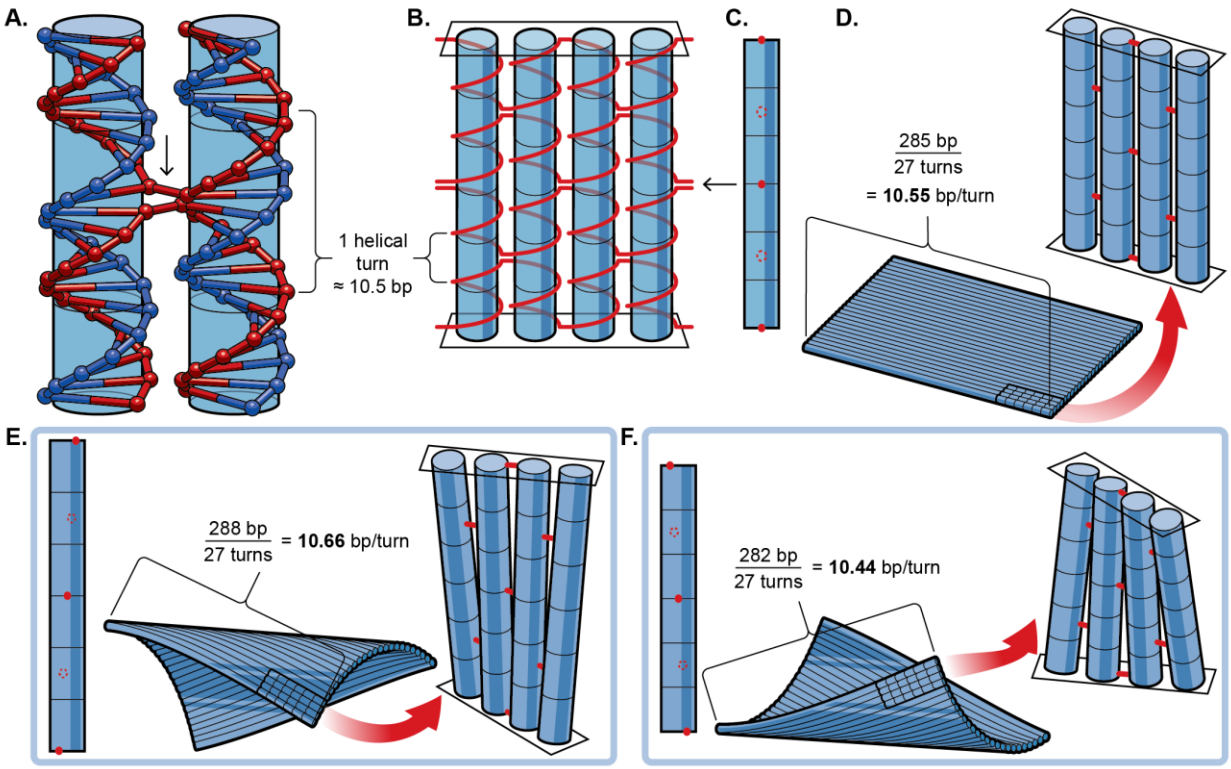

Figure 1. Crossover spacing between staple strands and DNA periodicity determine twist in DNA origami structures. A) Adjacent DNA helices joined by staple strand crossover (reciprocal antiparallel strand exchange) as in a DNA origami tile. Scaffold strand is indicated in blue. Two staple strands, indicated in red, both cross over to the adjacent helix at the cross-over site indicated by the arrow. B, C) In the complete DNA tile there exist multiple crossover sites, indicated in C) as red dots and circles corresponding to crossovers on either side of the helix. If the average crossover separation is commensurate with the periodicity of DNA (~10.5 bp/turn, indicated by black lines) then crossover sites will lie in a plane, binding parallel helices together to form a flat tile. D) A scheme for the synthesis of a near-flat tile (the 10.55 tile). Crossovers are positioned such that, if the tile is flat, 285 base pairs on each helix correspond to 27 helical turns, resulting in average helical pitch of 10.55 bp/turn. The original DNA origami tile[6] had 288 base pairs per helix, corresponding to an average pitch of 10.66 bp/turn if flat. This structure, when

relaxed, is predicted to have a global twist as shown in E). It is possible to twist the tile in the opposite direction by using a shorter crossover spacing as shown in F).

Small-angle X-ray scattering (SAXS) is a complementary technique for structural analysis that can be used to probe the shape of DNA origami nanostructures in solution. The method produces profiles of scattering intensity $I(q)$ as a function of the magnitude of the scattering wavevector $q = 4\pi sin\theta/\lambda$, where 2θ is the scattering angle and λ the X-ray wavelength. Structural features are manifest as diffraction patterns that arise from the coherent scattering of X-rays from the electrons of atoms within the target particle. The utility of SAXS for the analysis of DNA nanostructures has only recently been established. The first two studies demonstrated that SAXS data can provide a useful test of the validity of structural models of a DNA octahedron[24] and a DNA origami box.[7] SAXS has also been used to verify the formation of arrays of gold nanoparticles, connected through DNA octahedra.[25] Two recent papers extend these studies, further illustrating the power of SAXS for analyzing DNA nanostructures in solution. They demonstrate that repeated geometrical features of DNA origami such as the interhelical spacing result in clearly discernible diffraction peaks which can be used to quantify their internal geometry.[26] They also show that SAXS can quantify the equilibrium distribution of conformational states providing useful thermodynamic information,[26,27] including the dependence of the folding of DNA origami structures and interhelical spacing, on temperature and the concentration of magnesium ions.[26] The opportunity to perform time-resolved SAXS experiments at high-flux synchrotron beamlines has also been utilized to perform kinetic measurements on conformational transitions and dimerization of DNA origami structures with millisecond temporal resolution.[28]

There are, however, intrinsic challenges in the analysis of DNA origami structures with SAXS. In particular, sample requirements are stringent.[29] Samples need to be sufficiently pure and monodisperse that diffraction from the origami dominates the observed scattering. Moreover, sample concentrations must be sufficiently high that diffraction peaks corresponding to internal features of a DNA origami structure are visible. DNA origami nanostructures at concentrations as low as 0.1 mg/ml produce high signal-to-noise at low scattering angles[27] but the signal decays at the higher scattering angles which contain information on the internal structure of DNA origami: Fischer *et al.* used ~1.3 mg/ml of purified DNA origami nanostructures to quantify the interhelical spacing by resolving a corresponding diffraction peak at $q = \sim 0.23\,\text{Å}^{-1}$.[26] Although SAXS allows for the quantification of characteristic periodicities in DNA origami structures, SAXS data alone is insufficient to define global dimensions without *a priori* knowledge about the structure of the target particle. Absolute model-free distance measurements can be achieved by immobilising pairs of gold nanoparticles, which act as strongly scattering probes.[30-33] This approach has recently been used to measure the arrangement of immobilised gold nanoparticles on DNA origami.[34]

Here we demonstrate that SAXS can distinguish between single-layer DNA origami tiles designed to have different amounts of twist, even though when immobilised on a mica surface and imaged with AFM the tiles appear to have identical shapes. We use SAXS to explore the effect of crossover periodicity on the global twist of single-layer DNA origami structures. By comparing predicted scattering from finite-element (FE) models of twisted DNA tiles to experimental SAXS data, we show that the global twist in single-layer DNA origami is much more sensitive to staple crossover periodicity than has been previously observed in multi-layer DNA origami structures.[13] We then address the challenge of making direct measurements of the

overall dimensions of DNA origami structures by using gold nanoparticles as fiducial marks. Finally, we demonstrate that, with sample concentrations as low as 0.1 mg/ml, SAXS can be used to measure characteristic dimensions of a DNA origami nanotube, including the interhelical spacing and the diameter of an individual double helix.

RESULTS/DISCUSSION

SAXS reveals structural features in solution that are not observable by AFM imaging. To test whether imaging with AFM can be used to measure the global twist of a DNA origami tile, we constructed a single-layer DNA origami tile with an average spacing between crossovers of 10.44 bp/turn, a smaller deviation from the unstrained DNA helix periodicity than in twisted multi-layer DNA origami previously studied.[13] We expected this '10.44 tile' to be over-wound when flat and therefore to twist in the opposite direction to Rothemund's original DNA origami tile[6] (Figure 2A). Additionally, we prepared two variants: a 'braced' tile consisting of the same structure modified with two pairs of bracing DNA helices running across the surface, perpendicular to the DNA helices of the tile (Figure 2B), an attempt to flatten the tile and reduce any global twist; and a 'rolled' tile, with modified staples that were designed to join opposite edges to roll the tile into a tube (Figure 2C). These designs are detailed in Figure S1. We compared their structures when immobilized on a mica surface, imaged with AFM, and in solution, probed with SAXS. AFM images of all three tiles have the same overall shape and dimensions. The perpendicular braces are visible in images of the braced tile and a small fraction of the rolled tiles (3 out of 236 examples imaged) appear to be rolled into a tube which has been flattened on the surface (Figure 2D-F, Figure S2). In contrast, the SAXS scattering profiles for each tile type are clearly distinguishable and can be used to infer differences between the shapes of the tiles in solution. Scattering from all tile types displays a broad peak (Figure 2G). The rolled tile gives rise to the most prominent peak at the largest q-value (~ 0.032 Å^{-1}), indicative of the most compact structure. The peak in the scattering data for the braced tile shows the least prominent peak at the smallest q-value (~ 0.020 Å^{-1}), indicative of the most extended structure. Scattering from the unmodified tile is intermediate, with a peak at $q \approx 0.025$ Å^{-1} (Figure 2G).

Differences between scattering data from each tile type are also clearly apparent in superimposed log(I) vs q and log(I) vs log(q) plots over an extended q range (Figure S3). This behavior is in agreement with calculated scattering from a series of model tiles with different curvatures, for which the first scattering peak becomes less pronounced and moves to lower q as curvature decreases (Figure S4). The braced tile is also most consistent with an analytical solution of scattering from a geometric model with theoretical dimensions of a flat tile (Figure S3). SAXS data thus demonstrates that the structures of these tiles differ in solution: the braced tile is the flattest and the rolled tile is the most compact.

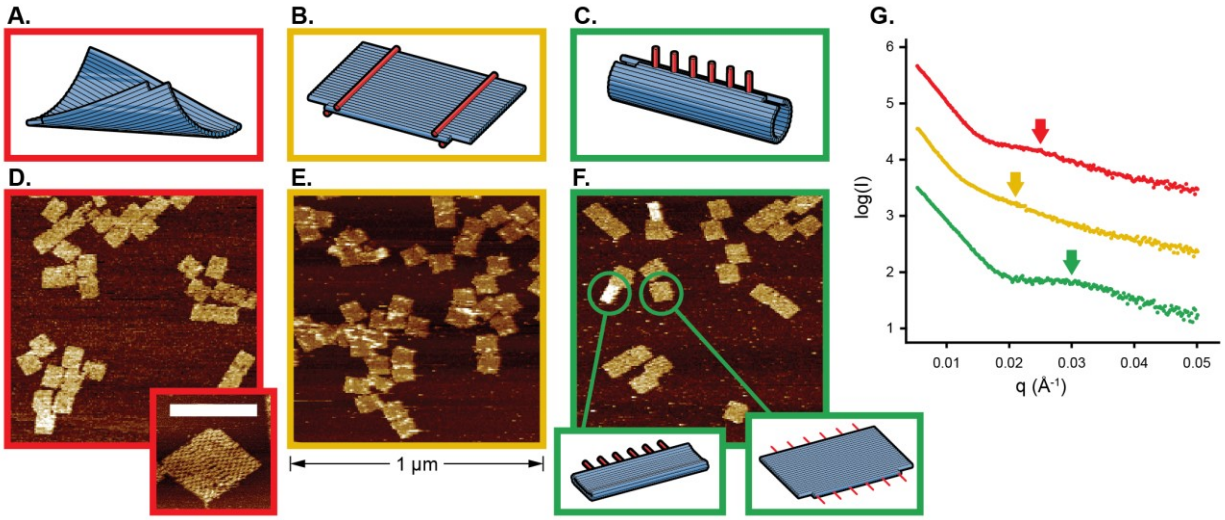

Figure 2. Comparison of DNA origami tiles imaged on a surface with AFM and in solution with SAXS. A)-C) Diagrams of the unmodified 10.44 (A), braced (B), and rolled (C) tiles, with modifications to the braced and rolled tiles indicated in red. D)-F) AFM images for unmodified (D), braced (E) and rolled (F) tiles respectively (field of view 1 µm x 1 µm; see Figure S2 for full images). Inset in D is a magnified image of a single tile in which individual helices can be resolved (scale bar 100 nm). In (F), representative examples of rolled (N = 3) and opened (N = 233) tile are circled in green. (G) Small-angle X-ray scattering data for the unmodified (red),

braced (yellow), and rolled (green) tiles respectively. The first scattering peak is indicated in each case.

The effect of crossover periodicity on single-layer DNA origami. To determine the effect of small deviations between crossover and DNA helix periodicity on single-layer DNA origami, we collected SAXS data from unbraced DNA tiles with three average crossover periodicities corresponding to 10.44, 10.55 and 10.66 bp/turn for a flattened tile (referred to as 10.44, 10.55 and 10.66 tiles respectively); cadnano designs are in Figures S1A and S5. The 10.44 and 10.66 tiles produce clear diffraction peaks whereas diffraction peaks from the 10.55 tile are substantially less pronounced (Figure 3). To resolve the shape of the tiles in solution we compared experimental data to theoretical SAXS profiles. These were calculated from 29 coarse-grained FE models of tiles with varying degrees of global twist that were generated using the structural modelling program CanDo.[35] The more twisted tiles adopt a tubular shape and produce more pronounced diffraction peaks than flatter tiles (Figure S4). The strong diffraction features in the 10.44 and 10.66 tiles allow unambiguous identification of the best-fitting structural model (Figure S6), which produces diffraction features that align well with experimental data, plotted in Figure 3. As an indication of the sensitivity of the fit to the twist of the tile, theoretical scattering from models with slightly different degrees of global twist ($\pm$ 14° deg/tile) are also plotted. These nearby models produce scattering peaks which are clearly not in alignment with the experimental data. From the best-fit models, we estimate that in solution, tiles with average crossover periodicities consistent with 10.44 and 10.66 bp/turn for a flattened tile are twisted by 180° over a distance of 120 nm, presumably in opposite directions although SAXS data cannot distinguish between the handedness of the twist (Figure S7). By comparison, multi-layer DNA

origami structures with crossover periodicities of 10 and 11 bp per turn (deviating from the nominal periodicity of a DNA helix by +/- 0.5 bp per turn) have been observed to twist by 180° in 235 ± 32 nm and 286 ± 48 nm respectively.[13] Our data show that single-layer structures are much more sensitive to crossover periodicity, enabling a more precise estimate of the relaxed average periodicity of DNA helices in an origami. The similar magnitude of the opposite twists of the 10.44 and 10.66 tiles suggests that a tile designed with an average periodicity of 10.55 bp per turn would be approximately flat (although the asymmetry of the tile, which was designed such that all staple ends are positioned on the same face, may mean that its twist is not symmetrically sensitive to over- and underwinding). The 10.55 tile is indeed flatter: a geometric model of a flat sheet is consistent with the lack of clear diffraction peaks in the 10.55 tile but not the strong diffraction features of the 10.44 and 10.66 tiles (Figure S7). Moreover, the best fitting model tile has a lower global twist and all flatter tile models fit similarly well to experimental data (Figure S6). For comparison, scattering from the best-fitting tile and a completely flat tile are shown overlaid with experimental scattering from the 10.55 tile in Figure 3.

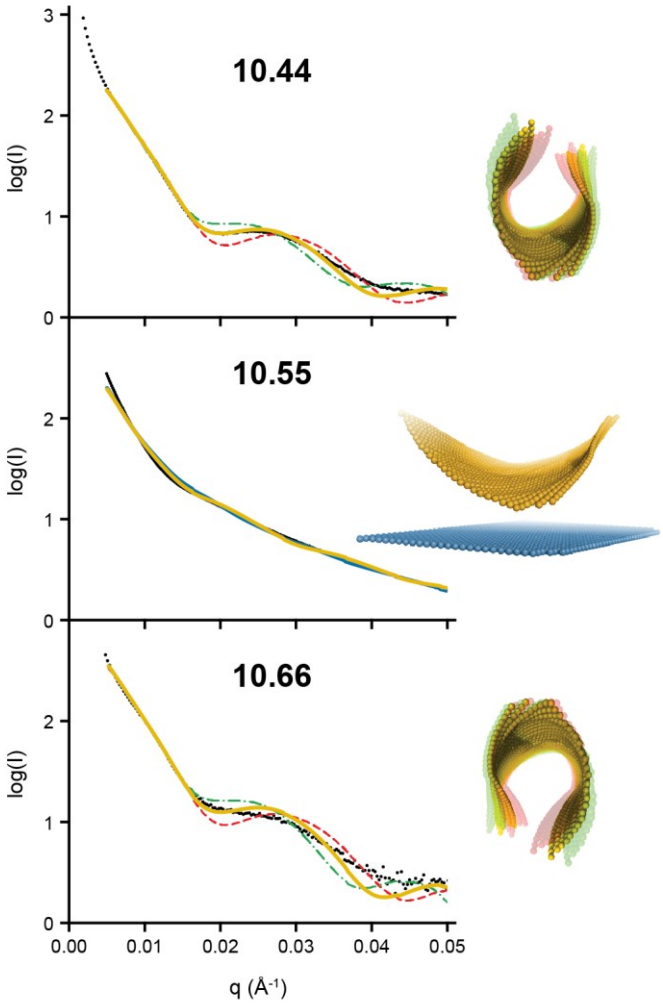

Figure 3. Effect of crossover periodicity on the global twist of the DNA origami tile. Experimental scattering (black circles) for 10.44 tile (top), 10.55 tile (middle), and 10.66 tile (bottom). For each data set, the best-fitting theoretical scattering data (smallest root mean squared deviation) from the set of model tiles (Figure S4) is overlaid (yellow line). For the 10.44 and 10.55 tile, theoretical scattering from model tiles that are less twisted (red dashes) and more twisted (green dot-dashes) is also overlaid (± 14˚/tile global twist). The corresponding model structures are shown on the right. For the 10.55 tile (middle), the structure and calculated scattering for the completely flat model tile is displayed in blue for comparison.

Measuring distances between reference points on a DNA origami in solution using immobilised gold nanoparticles. We used SAXS to measure distances between pairs of gold nanoparticles of 55 ± 8 Å diameter tethered to specific locations near corners of the 10.44 tile (Figure S8). The ratio between the electron densities of gold and water is significantly greater than that between DNA and water (approximately 14 and 2, respectively).[36] Scattering intensity is proportional to the square of the contrast in electron density between the scattering particle and solvent.[36] Thus, scattering from the pair of gold nanoparticles, which contains information about their size and the distance separating them, is readily observable in SAXS data. Scattering intensities from the 10.44 tile, unlabelled and labelled with either one or a pair of gold nanoparticles, are shown in Figure 4A. Scattering from doubly- or singly-labelled tiles closely resembles scattering from a control suspension of gold nanoparticles, indicating that scattering from the gold labels dominates that from the origami, as expected. Small, approximately evenly spaced peaks at small wavevector magnitudes $q < 0.05\ \text{Å}^{-1}$ are observable in SAXS data from tiles with gold pairs. These are absent in scattering from tiles labelled with a single gold particle and from unlabelled tiles. We attribute these features to coherent scattering from pairs of gold nanoparticles immobilized on the same tile, for which we expect intensity maxima close to those of the function $\sin(qd)/qd$ where d is the distance between the gold pairs. By fitting these small-angle peaks (Figure S9) we estimate that d = 819 Å, 95% CI = (814 Å, 823 Å).

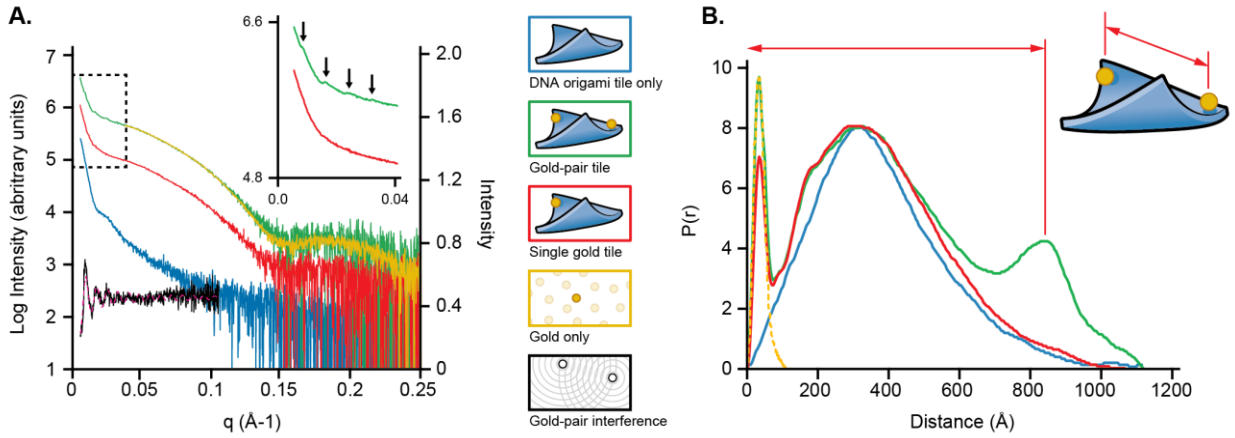

Figure 4. Measuring distances between reference points using pairs of immobilised gold nanoparticles. (A) Scattering intensities and (B) fitted pair distance distribution functions from the 10.44 tile, either unlabelled (blue), labelled with a single gold nanoparticle (red) or a pair of nanoparticles (green). Corresponding data for a suspension of free gold nanoparticles (yellow) is shown for comparison. Inset in (A) is an enlargement of scattering intensities from gold-labelled tiles within the region encircled by a dotted rectangle; arrows point to regular diffraction features seen only in tile labelled with pairs of gold nanoparticles. Black data in (A) is a linear combination of scattering spectra that depends on the interference between scattering from pairs of immobilised gold nanoparticles (Figure S9): this was fitted to the function $1 + 2 \times sin(qd)/qd$ to estimate d, the distance between pairs of gold nanoparticles.

Information on the structure of the scattering particles can also be derived from SAXS data using an indirect Fourier Transform method[37] implemented in the software GNOM.[38] This computes a real-space electron pair distance distribution function $P(r)$ for which the calculated scattering is consistent with SAXS data; it is frequently used for the interpretation of SAXS from biological samples.[29] The $P(r)$ function derived from SAXS data for the unmodified DNA tile (Figure 4B) has a single, broad peak with maximum at approximately 300 Å. For gold-labelled tiles, the

calculated $P(r)$ has a similar peak which is slightly broader and has a shoulder at approximately 180 Å; we attribute these shape changes to density correlations between the tile and gold labels (leading to interference between scattering from these components), and possibly to distortion of the tile by the labels. An additional prominent peak at 33 Å in $P(r)$ for both sets of labelled tiles matches the sharp peak in $P(r)$ calculated from scattering from a suspension of gold nanoparticles: it originates from density correlations within a single gold particle. This peak is observed at a larger distance than expected for a uniform 55 Å sphere, for which $P(r)$ is maximal at 29 Å:[37] we attribute this increase in apparent nanoparticle size to the additional electron density contributed by the coating of thiolated T_{15} oligonucleotides. A second additional peak is observed in $P(r)$ for the doubly gold labelled tile only; we attribute this to density correlations between the two gold nanoparticle labels. This feature has a maximum at 828 Å which is close to the particle spacing deduced from the same data by the alternative analysis presented above (Figure S9). The second peak is expectedly broader, but its width cannot be explained by the particle size alone and is likely contributed to by flexibility in the AuNP anchor[34] or the DNA origami structure or both.

These results indicate that the distance between immobilised pairs of gold nanoparticles is slightly shorter than the expected separation between their binding sites for a flat tile (~855 Å) but longer than the distance calculated from the FE model that best fits the SAXS data from the 10.44 tile (~750 Å) (Figure S8). Gold nanoparticles have previously been used in SAXS experiments to measure distances on a range of nucleotide structures. These include for determining the length distributions of double stranded DNA[30,31] more recently with anomalous scattering,[33] to probe conformational changes induced by the *Escherichia coli* mismatch repair system,[39] the solution conformations of RNA kink-turn motifs,[32] to quantify the repeat distance

in 2D arrays[33] and chiral arrangements of nanoparticles on DNA origami.[34] Here, we have demonstrated the use of gold nanoparticles as fiducial markers to measure much longer distances, well beyond the range of alternative Förster resonance energy transfer methods (typically less than 100 Å),[40] on a DNA origami structure.

Resolving the internal structure of DNA nanotubes. Previous studies have demonstrated that prominent periodicities such as the inter-helical spacing in DNA origami nanostructures can be inferred directly from peaks in SAXS scattering data.[26] However, SAXS data from structures that are flexible (such as single-layer origami) or that have more than one closely-separated characteristic distance may not be readily deconvolved into a small number of well-defined peaks. Here, we extend the use of indirect Fourier methods to determine the internal structure of a single-layer, rotationally symmetric, DNA origami nanotube comprising 10 DNA helices [41] (Figure S10). Experimental scattering data from DNA nanotubes were compared to the theoretical scattering profiles for a set of atomic models with a range of tube diameters (80 Å – 120 Å). The atomic model with a 95 Å diameter provided the best fit to the experimental scattering (Figure 5A and 5B), significantly better than for atomic models with diameters deviating by ±10 Å. SAXS data was also well described by analytical solutions to a hollow cylinder with a diameter of 95.6 ± 0.3 Å and wall thickness of 23.4 ± 0.4 Å, which is consistent with the width of a DNA duplex (Figure S12). Analytical models also demonstrated how sharp dips in model compared to experimental data can be accounted for by allowing for size dispersion in the diameter (Figure S12).

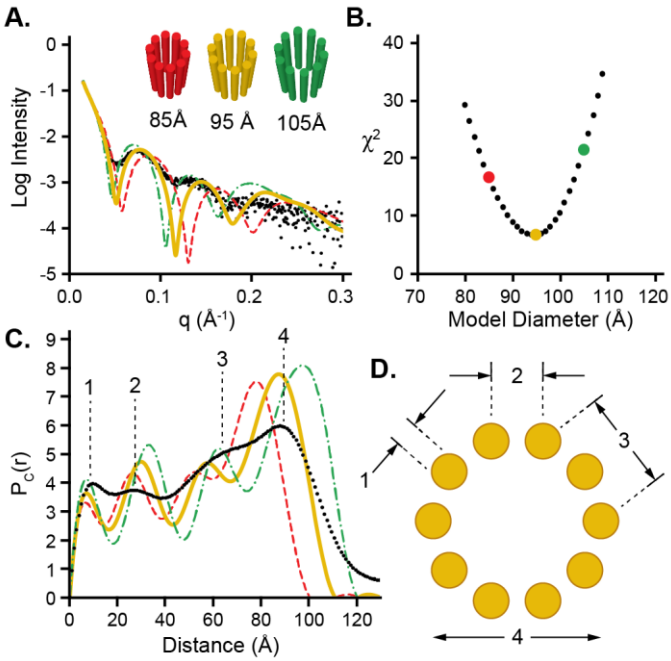

Figure 5. Analysis of SAXS data from DNA origami nanotubes. A) Experimental SAXS for 10-helix DNA nanotube (black circles) overlaid with the theoretical scattering from the best-fitting model nanotube (95 Å diameter, yellow line). Nearby models are indicated for comparison (85 Å diameter, red dashed; 105 Å diameter, green dot-dashed). B) χ^2 Goodness-of-fit residuals between experimental scattering and simulated scattering for model barrels of various diameters. Coloured circles indicate model barrels plotted in A. C) Cross-sectional *P(r)* inferred from experimental data and for models shown in A. D) Cross-section of model nanotube indicating characteristic distances corresponding to peaks in *P(r)*.

The nanotube is an elongated particle (approximately 100 Å × 2100 Å) with consistent cross-section. It is also likely to be rigid in solution since it is far shorter than the reported persistence length of a 10 helix DNA nanotube of 15 μm.[42] The nanotube is therefore ideally suited for cross-sectional analysis with SAXS. For elongated particles scattering intensities are given by:

$$I(q) = \frac{l\pi}{q} I_c(q)$$

where l is the length of the particle and $I_c(q)$ depends only on its cross-sectional structure.[43] This allows the use of Fourier transform methods to derive a cross-sectional real-space pairwise distance distribution function ($P_c(r)$) for the DNA nanotube (Figure 5C and S12) and the cross-sectional radius of gyration, R_g = 48.2±0.3 Å which, for a thin cylinder, is equal to the radius. We thus estimate the mean diameter of the nanotube to be 96.3±0.6 Å, consistent with the diameters determined by fitting geometric models as described above and corresponding to an inter-helical spacing of 30 Å.

Experimental and model-generated $P_c(r)$ plots for the 10-helix barrel comprise 4 distinct peaks (Figure 5C). Experimental peaks are broader than those calculated for models comprising rigid, parallel helices. This may reflect flexibility of the tubes and the bending of helices within an origami structure in which interhelical distances are typically observed to be smallest at crossover locations.[6,21,44] By calculating $P_c(r)$ plots for pairs of parallel helices spaced at different distances, and for tubes with different diameters and numbers of helices (Figure S11), we were able to attribute the first (at 9.8 Å), second (at 27.5 Å) and third (at ~60 Å) peaks to coherent scattering from an individual helix, from neighbouring helices, and from next-nearest neighbour helices respectively. The fourth peak (at 88.2 Å) was attributed to scattering over the entire cross section of the tube. This occurs at a distance slightly smaller than the tube diameter. The inferred interhelical spacing of the single-layer DNA nanotube is comparable to that measured using SAXS from a 3D DNA origami lattice (26 Å).[26] The interpretation of diffraction peaks in scattering from structures lacking the regular lattice of a typical 3D origami can be difficult,[26] and concentrated samples may be necessary to provide adequate signal-to-noise. We

have shown that indirect Fourier methods provide an alternative approach to probing the internal geometry of non-lattice DNA origami structures, enabling quantitative analysis of dilute samples.

METHODS/EXPERIMENTAL

DNA origami synthesis and purification. Ten-fold excess (~2 μM) of each staple oligo (Integrated DNA Technologies) over scaffold DNA (M13mp18 ssDNA viral genome, Bayou Biolabs) were combined in synthesis buffer (33.0 mM Tris Acetate, 12.5 mM Mg Acetate, pH 8.3). DNA origami structures were synthesised in a single step by heating to 94˚C then cooling to 20˚C over 6 hours. Excess staples were then removed by size exclusion chromatography, with at least three passes through 350μL Sephracyrl S300 beads (GE Healthcare) equilibrated in synthesis buffer as previously described. [10]

Attachment of gold nanoparticles to DNA origami structures. Gold nanoparticles were attached to DNA tiles as previously described.[45,46] Briefly, 5.5 nm gold nanoparticles (Nanopartz, Batch No. 16216) were first concentrated by precipitation by addition of NaCl, then coated with Bis(p-sulfonatophenyl)phenylphosphine dihydrate dipotassium salt (BSPP) (Sigma-Aldrich) by first resuspending in 1 mM BSPP and 50% methanol, then pelleting and resuspending again in 2.5 mM BSPP in water. Following this, poly-T oligonucleotides functionalized with a sulfhydryl group at the 5’ end were coupled to the surface of gold nanoparticles by incubating gold particles in 75 fold molar excess of 5’-thiolated DNA (T_{15}-SH) for two days at room temperature in 1×TBE (10 mM Tris-HCl, 1mM EDTA). Excess thiolated DNA was removed immediately prior

to coupling to DNA origami structures with four passes through a 100 kDa centrifugal filter (Amicon).

To couple poly-T-coated gold nanoparticles to DNA origami structures, a 50-fold molar excess of gold nanoparticles was incubated with purified DNA origami nanostructures with three poly-A staple extensions per gold nanoparticle, spaced approx. 6 nm apart and centred around each desired gold binding site. The mixture was incubated for at least 24 hours at room temperature before excess gold nanoparticles were removed by three passes through 350µL Sephracyrl S300 beads equilibrated in synthesis buffer.

Atomic force microscopy. The origami sample was diluted to an appropriate concentration in 12.5 mM magnesium acetate and 1×Tris-acetate, pH 8.3 (40 mM Tris, 20 mM acetic acid), then purified before imaging by 3 rounds of filtration through Sephacryl S-300 resin, where the resin had been equilibrated in a buffer comprising 1×TE (10 mM Tris-HCl, 1mM EDTA, pH 8.0), 50 mM NaCl and 10 mM $MgCl_2$. A volume of a few µL of origami was deposited on freshly cleaved mica and allowed to adsorb. Atomic Force Microscope images were acquired using a Veeco Dimension 3100 in tapping mode in fluid. The imaging buffer contained 12.5 mM magnesium acetate, 4 mM $NiCl_2$, in 1×Tris-acetate, pH 8.3. Bruker SNL probes were used. Images were processed using Nanoscope Analysis; this involved flattening to second order and adjustment of the image contrast.

Small-angle X-ray scattering. SAXS data for the 10.44, 10.55 and 10.66 DNA origami tile as well as the 10 helix DNA origami nanotube were collected on the SAXS/WAXS Beamline at the Australian Synchrotron, Melbourne, Victoria. Samples at concentrations of ~0.1 mg/ml (equivalent to 20 nM) for unlabelled origami and ~ 0.05 mg/ml for gold-labelled origami, were

passed multiple times through a 1.5-mm quartz capillary at 20 °C, through which monochromatic X-rays (11 keV) were passed at a flux of 4×10^{12} photons per second. SAXS data were collected with exposure times of 5 s on a Pilatus 1M photon counting detector (Dectris), and scattering intensity I(q) was collected in the range of $0.0015 < q < 0.4$ Å^{-1}, where q=(4πsinθ)/λ, 2θ is the scattering angle and λ is the X-ray wavelength. SAXS data for comparing the unmodified, rolled and braced 10.44 DNA origami tile as well as with immobilized gold nanoparticles were collected at the European Molecular Biology Laboratory (EMBL) on the EMBL-P12 BioSAXS beamline at the PETRAIII storage ring (DESY, Hamburg) with a 2D photon counting pixel X-ray detector Pilatus 2M (Dectris, Switzerland). The scattering intensity, $I(q)$, was recorded in the range of $0.0054 < q < 0.55$ Å^{-1}. All data were collected in synthesis buffer.

Processing of SAXS data. SAXS data reduction was performed using beamline-specific software packages at the SAXS/WAXS beamline at the Australian Synchrotron and EMBL-P12 BioSAXS beamline at the PETRAIII storage ring. After removal of outlier frames resulting from air or meniscus in the capillary, sample datasets and buffer datasets (from synthesis buffer alone) were averaged. For all samples, including SAXS data from DNA origami structures with and without immobilised gold nanoparticles and colloidal gold nanoparticles, solvent blanks were subtracted before further processing. Data subtraction and scaling were performed using the software PRIMUS.[47] SAXS provides structural information from the shape of scattering profiles rather than their absolute intensities, which relates to several factors including sample concentration, molecular weight and beam flux. Thus, to aid comparison between the structure of target particles, all data were scaled between different datasets and scattering intensities presented in figures are in arbitrary units.

Generation of 3D structural models. A basis set of 29 tiles with increasing degrees of twist from a completely flat tile was generated as follows. A subset of tile models twisted to various degrees were generated using finite element modeling by entering DNA origami tile design files with different crossover spacing and by altering the input 'DNA periodicity' parameter in the program CanDo.[35] This produced 3D models of twisted tiles where each DNA helix was represented as a set of cylinders. These were converted into 'dummy atom' models, which were formatted as protein databank (PDB) files so that theoretical scattering could be calculated using the software FOXS.[48] In dummy atom models, DNA helices were represented as arrays of spheres with diameter 22.5 Å, positioned side-by-side along the helical axis. However, models generated from CanDo provided a coarse sampling over a range of twist magnitudes. For a finer sampling, we generated models of intermediate twist states by linearly interpolating coordinates between structures from CanDo outputs. The global twist in model tiles was calculated by summing the local pitch at the position of each dummy atom. The local pitch was calculated by measuring the dihedral angle defined by all sets of four adjacent dummy atoms as illustrated in Figure S4C.

DNA nanotubes were constructed using the molecular modelling software The PyMOL Molecular Graphics System, Version 1.8 (Schrödinger, LLC) as atomic models consisting of 10 ideal B-DNA helices, each 2100 Å in length, arranged as described in Figure S11. From these PDB files, we generated theoretical scattering using FOXS. [48]

Model fitting to scattering data. The fit between model and experimental data were quantified using the reduced χ^2 error weighted scoring function[48,49] $\chi^2 = \frac{1}{M}\sum_{i=1}^{M}\left(\frac{I_{exp}(q_i) - I_{model}(q_i)}{\sigma(q_i)}\right)^2$ over $0.01\,\text{Å}^{-1} < q < 0.05\,\text{Å}^{-1}$ for the DNA tiles and for $0.015\,\text{Å}^{-1} < q < 0.3\,\text{Å}^{-1}$ for DNA nanotubes.

Analytical models were fit to experimental SAXS data using SasView v4.1.2 (http://www.sasview.org).

Calculation of Distance Probability Distributions. GNOM (ATSAS v2.7.1) was used to calculate pairwise distance distribution functions from scattering profiles with indirect Fourier methods.[38] For real-space cross-sectional analysis of the DNA origami barrels, the range $0.0\,\text{Å}^{-1} < q < 0.3\,\text{Å}^{-1}$ was used with R_{min} restrained to 0. Since D_{max} is an ill-defined parameter in pairwise distance distribution functions, we examined the effect on peak positions at different D_{max} values between 50 and 200 Å at 10 Å resolution. The peak positions remained similar above a threshold D_{max} of 120 Å and the peak values of the $P_c(r)$ distributions varied by less than 2 Å between 120 and 200 Å. Therefore, D_{max} for both experimental and model $P_c(r)$ curves were set to 200 Å in Figure 5C and Figure S11 and for calculation of sum χ^2 goodness of fits between experimental and model data. 200 Å was sufficient to account for the maximal cross-sectional distance in the DNA nanotube model with the largest outer diameter. For all models, the pairwise distance distribution approached 0 where r was equal to the maximal cross sectional diameter of the model. For the final experimental $P_c(r)$ plot from which structural parameters such as R_g were calculated, the D_{max} was set to D_{max}=146 Å because this resulted in the highest scoring fits between $P_c(r)$ plots and scattering data. $P_c(r)$ and $P(r)$ plots were scaled for comparison. Subsequently, units presented in figures are arbitrary.

Transmission electron microscopy of DNA Nanotube. DNA nanotube solution (2 µL, 10nM in TAE consisting of 40 mM Tris-acetate and 1 mM EDTA, pH 8.3) was drop cast onto carbon/formvar-coated copper grids and left to adsorb for five minutes before excess liquid was wicked away with filter paper. Samples were negatively stained with 2% (w/v) uranyl acetate in water for two minutes. Excess stain was similarly wicked with filter paper and the grids dried

overnight. Imaging was performed with a Tecnai G2 20 Transmission Electron Microscope (FEI) in bright-field mode at 200 keV.

AUTHOR CONTRIBUTIONS

M.A.B.B. and A.J. Tuckwell prepared samples, collected, processed and analyzed SAXS data, and wrote the manuscript. J.F.B. analyzed SAXS data and wrote the manuscript, J.B. and F.B. designed DNA nanotubes, A.P.D. and A.E.W. analyzed SAXS data, K.E.D. performed AFM imaging, R.M.H. collected SAXS data, A.J. Turberfield designed the project and wrote the manuscript, L.K.L. designed the project, prepared samples, collected, processed and analyzed SAXS data and wrote the manuscript

ACKNOWLEDGMENT

We would like to acknowledge the assistance and support of staff and beamline scientists at on the SAXS/WAXS beamline at the Australian Synchrotron, Victoria, Australia, and at the P12 beamline at the PETRA storage ring at EMBL-P12 BioSAXS beamline at the PETRAIII storage ring in DESY Hamburg. We would also like to thank Cy Jeffries for useful discussions on data analysis and Emeline Vernhes for her technical assistance with the design and SAXS data collection on the DNA origami tiles. This work benefited from the use of the SasView application, originally developed under NSF award DMR-0520547. SasView contains code developed with funding from the European Union's Horizon 2020 research and innovation program under the SINE2020 project, grant agreement No 654000.

FUNDING SOURCES

This work was supported by the Australian Research Council (Grant DP130102219, L.L), the Human Frontiers Science Program (Grant RGP0030/2013 (L.K.L, A.J.T and J.B), the Engineering and Physical Sciences Research Council (grants EP/G037930/1, EP/P504287/1), and the Biotechnology and Biological Sciences Research Council (grants BB/H000321/1, BB/J00054X/1). A.J.T. was supported by a Royal Society–Wolfson Research Merit Award and L.K.L was supported by the Australian Research Council Discovery Early Career Research Award (Grant DE140100262).

Supporting information available: 12 supplementary figures showing cadnano designs of all DNA origami structures; full AFM micrographs; SAXS scattering data with extended q ranges, plotted superimposed and as log(I) vs log(q); fitted analytical solutions to SAXS data; theoretical scattering and pitch of dummy atom models of twisted tiles and χ^2 deviation from fits to SAXS data; schematic depiction of location of gold nanoparticles on DNA tile; details on determining distance between gold particle pairs in reciprocal space; simulations showing effect of interhelical spacing and diameter on pairwise distance distribution function of DNA nanotubes. This material is available free of charge *via* the Internet at http://pubs.acs.org.

REFERENCES

(1) Seeman, N. C. DNA in a Material World. *Nature* **2003**, *421*, 427–431.

(2) Chen, J. H.; Seeman, N. C. Synthesis From DNA of a Molecule with the Connectivity of a Cube. *Nature* **1991**, *350*, 631–633.

(3) Shih, W. M.; Quispe, J. D.; Joyce, G. F. A 1.7-Kilobase Single-Stranded DNA That Folds Into a Nanoscale Octahedron. *Nature* **2004**, *427*, 618–621.

(4) Goodman, R. P.; Schaap, I. A. T.; Tardin, C. F.; Erben, C. M.; Berry, R. M.; Schmidt, C.

F.; Turberfield, A. J. Rapid Chiral Assembly of Rigid DNA Building Blocks for Molecular Nanofabrication. *Science* **2005**, *310*, 1661–1665.

(5) Winfree, E.; Liu, F.; Wenzler, L. A.; Seeman, N. C. Design and Self-Assembly of Two-Dimensional DNA Crystals. *Nature* **1998**, *394*, 539–544.

(6) Rothemund, P. W. K. Folding DNA to Create Nanoscale Shapes and Patterns. *Nature* **2006**, *440*, 297–302.

(7) Andersen, E. S.; Dong, M.; Nielsen, M. M.; Jahn, K.; Subramani, R.; Mamdouh, W.; Golas, M. M.; Sander, B.; Stark, H.; Oliveira, C. L. P.; Pedersen, J. S.; Birkedal, P.; Besenbacher, F.; Gothelf, K. V.; and Kjems J. Self-Assembly of a Nanoscale DNA Box with a Controllable Lid. *Nature* **2009**, *459*, 73–76.

(8) Yurke, B.; Turberfield, A. J.; Mills, A. P.; Simmel, F. C.; Neumann, J. L. A DNA-Fuelled Molecular Machine Made of DNA. *Nature* **2000**, *406*, 605–608.

(9) Omabegho, T.; Sha, R.; Seeman, N. C. A Bipedal DNA Brownian Motor with Coordinated Legs. *Science* **2009**, *324*, 67–71.

(10) Wickham, S. F. J.; Bath, J.; Katsuda, Y.; Endo, M.; Hidaka, K.; Sugiyama, H.; Turberfield, A. J. A DNA-Based Molecular Motor That Can Navigate a Network of Tracks. *Nat. Nanotechnol.* **2012**.

(11) Green, S. J.; Bath, J.; Turberfield, A. J. Coordinated Chemomechanical Cycles: a Mechanism for Autonomous Molecular Motion. *Phys. Rev. Lett.* **2008**, *101*, 238101.

(12) Muscat, R. A.; Bath, J.; Turberfield, A. J. A Programmable Molecular Robot. *Nano Lett.* **2011**, *11*, 982–987.

(13) Dietz, H.; Douglas, S. M.; Shih, W. M. Folding DNA Into Twisted and Curved Nanoscale Shapes. *Science* **2009**, *325*, 725–730.

(14) Gerling, T.; Wagenbauer, K. F.; Neuner, A. M.; Dietz, H. Dynamic DNA Devices and Assemblies Formed by Shape-Complementary, Non-Base Pairing 3D Components. *Science* **2015**, *347*, 1446–1452.

(15) Binnig, G.; Quate, C. F.; Gerber, C. Atomic Force Microscope. *Phys. Rev. Lett.* **1986**, *56*, 930–933.

(16) Douglas, S. M.; Dietz, H.; Liedl, T.; Högberg, B.; Graf, F.; Shih, W. M. Self-Assembly of DNA Into Nanoscale Three-Dimensional Shapes. *Nature* **2009**, *459*, 414–418.

(17) Mitchell, J. C.; Harris, J. R.; Malo, J.; Bath, J.; Turberfield, A. J. Self-Assembly of Chiral DNA Nanotubes. *J. Am. Chem. Soc.* **2004**, *126*, 16342–16343.

(18) Malo, J.; Mitchell, J. C.; Vénien-Bryan, C.; Harris, J. R.; Wille, H.; Sherratt, D. J.; Turberfield, A. J. Engineering a 2D Protein-DNA Crystal. *Angew. Chem. Int. Ed. Engl.* **2005**, *44*, 3057–3061.

(19) Ke, Y.; Voigt, N. V.; Gothelf, K. V.; Shih, W. M. Multilayer DNA Origami Packed on Hexagonal and Hybrid Lattices. *J. Am. Chem. Soc.* **2012**, *134*, 1770–1774.

(20) Kato, T.; Goodman, R. P.; Erben, C. M.; Turberfield, A. J.; Namba, K. High-Resolution Structural Analysis of a DNA Nanostructure by cryoEM. *Nano Lett.* **2009**, *9*, 2747–2750.

(21) Bai, X.-C.; Martin, T. G.; Scheres, S. H. W.; Dietz, H. Cryo-EM Structure of a 3D DNA-Origami Object. *Proc. Natl. Acad. Sci. U. S. A.* **2012**, *109*, 20012–20017.

(22) Dubochet, J.; Booy, F. P.; Freeman, R.; Jones, A. V.; Walter, C. A. Low Temperature Electron Microscopy. *Annu. Rev. Biophys. Bioeng.* **1981**, *10*, 133–149.

(23) He, Y.; Ye, T.; Su, M.; Zhang, C.; Ribbe, A. E.; Jiang, W.; Mao, C. Hierarchical Self-Assembly of DNA Into Symmetric Supramolecular Polyhedra. *Nature* **2008**, *452*, 198–

201.

(24) Andersen, F. F.; Knudsen, B.; Oliveira, C. L. P.; Frøhlich, R. F.; Krüger, D.; Bungert, J.; Agbandje-McKenna, M.; McKenna, R.; Juul, S.; Veigaard, C.; Koch, J.; Rubinstein, J. L.; Guldbrandtsen, B.; Hede, M. S.; Karlsson, G.; Andersen, A. H.; Pedersen, J. S.; Knudsen, B. R. Assembly and Structural Analysis of a Covalently Closed Nano-Scale DNA Cage. *Nucleic Acids Res.* **2008**, *36*, 1113–1119.

(25) Tian, Y.; Wang, T.; Liu, W.; Xin, H. L.; Li, H.; Ke, Y.; Shih, W. M.; Gang, O. Prescribed Nanoparticle Cluster Architectures and Low-Dimensional Arrays Built Using Octahedral DNA Origami Frames. *Nat. Nanotechnol.* **2015**, *10*, 637–644.

(26) Fischer, S.; Hartl, C.; Frank, K.; Rädler, J. O.; Liedl, T.; Nickel, B. Shape and Inter-Helical Spacing of DNA Origami Nanostructures Studied by Small Angle X-Ray Scattering. *Nano Lett.* **2016**, acs.nanolett.6b01335.

(27) Bruetzel, L. K.; Gerling, T.; Sedlak, S. M.; Walker, P. U.; Zheng, W.; Dietz, H.; Lipfert, J. Conformational Changes and Flexibility of DNA Devices Observed by Small-Angle X-Ray Scattering. *Nano Lett.* **2016**, *16*, 4871–4879.

(28) Bruetzel, L. K.; Walker, P. U.; Gerling, T.; Dietz, H.; Lipfert, J. Time-Resolved Small-Angle X-Ray Scattering Reveals Millisecond Transitions of a DNA Origami Switch. *Nano Lett.* **2018**, *18*, 2672–2676.

(29) Jacques, D. A.; Trewhella, J. Small-Angle Scattering for Structural Biology-Expanding the Frontier While Avoiding the Pitfalls. *Protein Science* **2010**, *19*, 642–657.

(30) Mathew-Fenn, R. S.; Das, R.; Silverman, J. A.; Walker, P. A.; Harbury, P. A. B. A Molecular Ruler for Measuring Quantitative Distance Distributions. *PLoS One* **2008**, *3*, e3229.

(31) Mathew-Fenn, R. S.; Das, R.; Harbury, P. A. B. Remeasuring the Double Helix. *Science* **2008**, *322*, 446–449.

(32) Shi, X.; Huang, L.; Lilley, D. M. J.; Harbury, P. B.; Herschlag, D. The Solution Structural Ensembles of RNA Kink-Turn Motifs and Their Protein Complexes. *Nat. Chem. Biol.* **2016**, *12*, 146–152.

(33) Zettl, T.; Mathew, R. S.; Seifert, S.; Doniach, S.; Harbury, P. A. B.; Lipfert, J. Absolute Intramolecular Distance Measurements with Angstrom-Resolution Using Anomalous Small-Angle X-Ray Scattering. *Nano Lett.* **2016**, *16*, 5353–5357.

(34) Hartl, C.; Frank, K.; Amenitsch, H.; Fischer, S.; Liedl, T.; Nickel, B. Position Accuracy of Gold Nanoparticles on DNA Origami Structures Studied with Small-Angle X-Ray Scattering. *Nano Lett.* **2018**, *18*, 2609–2615.

(35) Kim, D. N.; Kilchherr, F.; Dietz, H.; Bathe, M. Quantitative Prediction of 3D Solution Shape and Flexibility of Nucleic Acid Nanostructures. *Nucleic Acids Res.* **2012**, *40*, 2862–2868.

(36) Svergun, D. I.; Koch, M. H. J.; Timmins, P. A.; May, R. P. *Small Angle X-Ray and Neutron Scattering From Solutions of Biological Macromolecules*; Oxford University Press, 2013.

(37) Glatter, O.; IUCr. A New Method for the Evaluation of Small-Angle Scattering Data. *J. Appl. Crystallogr.* **1977**, *10*, 415–421.

(38) Svergun, D. I.; IUCr. Determination of the Regularization Parameter in Indirect-Transform Methods Using Perceptual Criteria. *J. Appl. Crystallogr.* **1992**, *25*, 495–503.

(39) Hura, G. L.; Tsai, C.-L.; Claridge, S. A.; Mendillo, M. L.; Smith, J. M.; Williams, G. J.; Mastroianni, A. J.; Alivisatos, A. P.; Putnam, C. D.; Kolodner, R. D.; Tainer, J. A. DNA

Conformations in Mismatch Repair Probed in Solution by X-Ray Scattering From Gold Nanocrystals. *Proc. Natl. Acad. Sci. U. S. A.* **2013**, *110*, 17308–17313.

(40) Roy, R.; Hohng, S.; Ha, T. A Practical Guide to Single-Molecule FRET. *Nat. Methods* **2008**, *5*, 507–516.

(41) Benn, F.; Haley, N. E. C.; Lucas, A. E.; Silvester, E.; Helmi, S.; Schreiber, R.; Bath, J.; Turberfield, A. J. Chiral DNA Origami Nanotubes with Well-Defined and Addressable Inside and Outside Surfaces. *Angew. Chem. Int. Ed. Engl.* **2018**.

(42) Schiffels, D.; Liedl, T.; Fygenson, D. K. Nanoscale Structure and Microscale Stiffness of DNA Nanotubes. *ACS Nano* **2013**, *7*, 6700–6710.

(43) Glatter, O. Evaluation of Small-Angle Scattering Data From Lamellar and Cylindrical Particles by the Indirect Transformation Method. *J. Appl. Crystallogr.* **1980**, *13*, 577–584.

(44) Ke, Y.; Douglas, S. M.; Liu, M.; Sharma, J.; Cheng, A.; Leung, A.; Liu, Y.; Shih, W. M.; Yan, H. Multilayer DNA Origami Packed on a Square Lattice. *J. Am. Chem. Soc.* **2009**, *131*, 15903–15908.

(45) Sharma, J.; Chhabra, R.; Liu, Y.; Ke, Y.; Yan, H. DNA-Templated Self-Assembly of Two-Dimensional and Periodical Gold Nanoparticle Arrays. *Angew. Chem. Int. Ed. Engl.* **2006**, *45*, 730–735.

(46) Kuzyk, A.; Schreiber, R.; Fan, Z.; Pardatscher, G.; Roller, E.-M.; Högele, A.; Simmel, F. C.; Govorov, A. O.; Liedl, T. DNA-Based Self-Assembly of Chiral Plasmonic Nanostructures with Tailored Optical Response. *Nature* **2012**, *483*, 311–314.

(47) Konarev, P. V.; Petoukhov, M. V.; Volkov, V. V.; Svergun, D. I. ATSAS2.1, a Program Package for Small-Angle Scattering Data Analysis. *J. Appl. Crystallogr.* **2006**, *39*, 277–

286.

(48) Schneidman-Duhovny, D.; Hammel, M.; Tainer, J. A.; Sali, A. Accurate SAXS Profile Computation and Its Assessment by Contrast Variation Experiments. *Biophys. J.* **2013**, *105*, 962–974.

(49) Svergun, D.; Barberato, C.; Koch, M. H. J. CRYSOL– a Program to Evaluate X-Ray Solution Scattering of Biological Macromolecules From Atomic Coordinates. *J. Appl. Crystallogr.* **1995**, *28*, 768–773.